Chemical Engineering Journal 158 (2010) 353–361

Contents lists available at ScienceDirect

Chemical Engineering Journal

journal homepage: www.elsevier.com/locate/cej

Novel biodegradable chitosan–gelatin/nano-bioactive glass ceramic composite scaffolds for alveolar bone tissue engineering

Mathew Peter[a], N.S. Binulal[a], S.V. Nair[a], N. Selvamurugan[a,b], H. Tamura[c], R. Jayakumar[a,*]

[a] Amrita Centre for Nanosciences, Amrita Institute of Medical Sciences and Research Centre, Amrita Vishwa Vidyapeetham University, Elamakkara, Kochi 682026, Kerala, India
[b] Department of Biotechnology, School of Bioengineering, SRM University, Kattankulathur 603203, India
[c] Faculty of Chemistry, Materials and Bioengineering & High Technology Research Centre, Kansai University, Osaka 564-8680, Japan

ARTICLE INFO

Article history:
Received 9 October 2009
Received in revised form 25 January 2010
Accepted 1 February 2010

Keywords:
Chitosan
Gelatin
Bioactive glass ceramic nanoparticles
Nano-composite scaffolds
Alveolar bone tissue engineering

ABSTRACT

Bioactive glass ceramic nanoparticles (nBGC) were synthesized by sol–gel process and characterized using FTIR, TEM and XRD. Composite scaffolds of chitosan (CS)–gelatin (CG) with nBGC were prepared by blending of chitosan and gelatin with nBGC. The prepared CG/nBGC nano-composite scaffolds were characterized using FTIR, SEM and XRD. The effect of nBGC in the scaffold matrix was evaluated in terms of scaffold properties and biocompatibility. Our results showed macroporous internal morphology in the scaffold with pore size ranging from 150 to 300 μm. Degradation and swelling behavior of the nano-composite scaffolds were decreased, while protein adsorption was increased with the addition of nBGC. Biomineralization studies showed higher amount of mineral deposits on the nano-composite scaffold, which increases with increasing time of incubation. MTT assay, direct contact test, and cell attachment studies indicated that, the nano-composite scaffolds are better in scaffold properties and it provides a healthier environment for cell attachment and spreading. So, the developed nano-composite scaffolds are a potential candidate for alveolar bone regeneration applications.

1. Introduction

Alveolar bone loss is a common finding associated with periodontal degeneration [1]. Various treatment modalities have been used to regenerate or fill bony defects using different biomaterials like bioglass and hydroxyapatite. Guided tissue regeneration is one of the most commonly used clinical techniques to regenerate periodontal tissue. However the success rate of this technique is variable because of high susceptibility to infection which results in limited clinical improvement [2]. Cell based tissue engineering therapies are gaining more acceptance for regeneration of tissues. The goal of tissue engineering is reconstruction of living tissues with help of a biodegradable scaffolds for the purpose of replacement of damaged or lost tissue [3]. Tissue engineering requires the cells to have regenerative potential when seeded on three-dimensional networks that are implanted into the defect. Various synthetic and other biopolymers are used to construct scaffolds for tissue engineering applications [3]. Biopolymers have an advantage of being biodegradable and these materials contain structural groups similar to natural extracellular components.

Chitosan is a biopolymer derived from partial deacetylation of chitin. Chitosan is considered as an appropriate functional material for biomedical applications because of its high biocompatibility, biodegradability, non-antigenicity, antibacterial and blood coagulation properties [4–8]. The antibacterial properties [9] of chitosan makes it a suitable material for designing scaffolds for regeneration of alveolar bone since these areas are highly susceptible to bacterial infection. The ability of chitosan to support cell attachment and proliferation is attributed to its chemical properties. The polysaccharide backbone of chitosan is structurally similar to glycosaminoglycans, the major component of the extracellular matrix of bone and cartilage. Current attempts are focused on improving the mechanical and biological properties of chitosan scaffolds through the incorporation of bioceramics such as hydroxyapatite (HA) [10–12], β-tricalcium phosphate [13] and calcium phosphate [14], biomaterials like gelatin [15], alginate [16] or inorganic material such as montmorillonite [17]. The addition of bioceramics has been known to decrease resorption kinetics of the chitosan scaffolds [17]. The mechanical property increases with the addition of bioceramics in chitosan scaffolds.

Gelatin is a partial derivative of collagen and has been processed into composites by blending with other materials, such as chitosan, β-tricalcium phosphate (β-TCP) and hydroxyapatite (HA), for promoting cell attachment, migration, differentiation and proliferation. Gelatin is composed of a unique sequence of amino such as glycine, proline and hydroxyproline which promotes cell

* Corresponding author. Tel.: +91 484 2801234; fax: +91 484 2802020.
E-mail addresses: rjayakumar@aims.amrita.edu, jayakumar77@yahoo.com (R. Jayakumar).

1385-8947/$ – see front matter © 2010 Elsevier B.V. All rights reserved.
doi:10.1016/j.cej.2010.02.003

adhesion [18]. Gelatin concentration is known to influence the properties of the scaffold.

Bioactive glasses are osteoconductive and biodegradable biomaterials used for bone repair. It was developed by Hench [19] as a bone repair material. Recent studies have showed that degradation products of bioactive glasses could stimulate the production of growth factors, cell proliferation and activate the gene expression of osteoblast [20–25]. Bioactive glass can also bond to hard and soft tissues [26,27]. The bone bonding ability of the glasses has been attributed to their ability to form a surface layer of hydroxycarbonate apatite (HCA) [28]. Other studies showed that bioactive glasses are superior to hydroxyapatite coating on surface of implants [29]. Results of *in vivo* implantation show that these compositions produce no local or systemic toxicity, no inflammation, and no foreign-body response [30].

Sol–gel derived bioactive glasses tend to have more simple compositions than the melt-derived bioactive glasses and exhibit enhanced bioactivity and resorbability, due to a mesoporous texture inherent to the sol–gel process. Recently nano-bioactive glass ceramic has been synthesized by sol–gel process [31]. Webster et al. [32] revealed that the biomaterials in nano-scale could stimulate the reaction between materials and cells. Hence it would be interesting to study the effect of nBGC in nano-composite scaffolds, which has so far not been studied. This investigation focuses on the characterization of novel CG/nBGC nano-composite scaffolds for alveolar bone tissue engineering.

2. Materials and methods

2.1. Materials

Chitosan (Mw 100–150 kDa, degree of deacetylation-85%) was purchased from Koyo Chemical Co. Ltd. (Japan). Cow bone gelatin (Cat. No. 076-02765) was purchased from Wako Pure Chemical Industries, Ltd. (Osaka, Japan). Tetraethyl orthosilicate (TEOS), calcium nitrate ($Ca(NO_3)_2{\cdot}4H_2O$), citric acid, diammonium hydrogen phosphate, sodium borohydride, acetic acid, sodium hydroxide, bicinchoninic acid (BCA) reagents, minimum essential medium (MEM), 3-(4,5-dimethylthiazol-2-yl)-2,5-diphenyltetrazolium bromide MTT, Triton-X 100 HCl and isopropanol was purchased from Sigma–Aldrich Company. Glutaraldehyde (25% in water) and hen lysozyme were purchased from Fluka. Trypsin–EDTA (ethylenediaminetetraacetic acid) and fetal bovine serum (FBS) were obtained from Gibco, Invitrogen Corporation.

2.2. Preparation of bioactive glass ceramic nanoparticles (nBGC)

The procedure for preparing nBGC nanoparticles (SiO_2:CaO:P_2O_5 (mol%) ~ 55:40:5) is briefly described as follows: mixture A was prepared by adding 7.639 g of calcium nitrate to 9.84 ml of TEOS. This mixture A was then dispersed in a mixture containing ethanol and water (1:2 (mol)). The pH of mixture was adjusted in the range of 1–2 by adding citric acid and the mixture was stirred until a transparent mixture B was obtained. A second mixture C was prepared by adding 1.078 g of diammonium hydrogen phosphate and 15 g of poly(ethylene glycol) (PEG Mw 20,000) into 1500 ml deionised water and then the pH of the mixture was adjusted to 10 with ammonium water. Mixture B was then dropped into mixture C under vigorous stirring and the reaction mixture were aged for 24 h at room temperature to obtain a white gel precipitate. This precipitate was washed and filtered. The filtrate was then lyophilized to obtain a fine powder, which was calcinated at 700 °C to obtain nBGC nanoparticles (Fig. 1a).

2.3. Preparation of nano-composite scaffolds

Chitosan 2% (w/v) was dissolved in 1% acetic acid solution. Gelatin was added into chitosan solution and stirred for 12 h at 37 °C. Then nBGC (1 wt.%) was added into chitosan–gelatin (CG) mixture and stirred for 24 h. Resultant mixture was subjected to ultrasonication (Vibra cell VC 505) to further disperse and reduce particle size. 0.25% glutaraldehyde was added as a crosslinker. The resultant mixture was transferred into 12 well culture plates and pre-freezed at −20 °C for 12 h followed by freeze-drying (Christ alpha LD plus) at −80 °C for 48 h. Then the scaffolds were neutralized by 2% NaOH and 5% NaBr for 2 h and further washed with deionised water. Finally the scaffolds were freeze-dried and stored

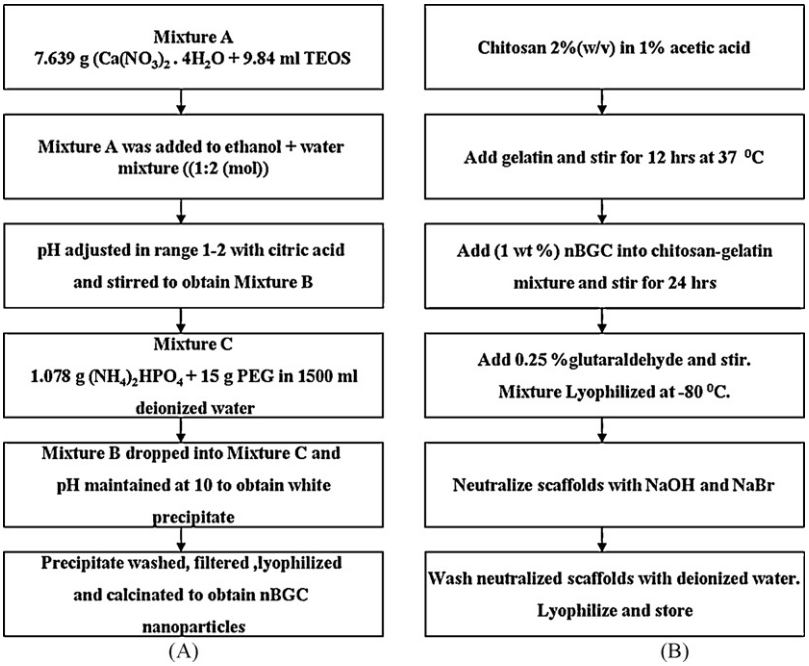

Fig. 1. (a) Flow chart showing the steps in the synthesis of nBGC nanoparticles and (b) shows the steps in preparation of composite scaffolds.

for further use. Three different concentrations (0.5, 1 and 2%, w/w) of CG mixture were prepared into which 1% nBGC was dispersed and then freezed dried to prepare the nano-composite scaffolds (Fig. 1b).

2.4. Characterization studies

The morphology and size of nBGC was assessed using TEM. nBGC was dispersed in ethanol and TEM images were taken using JEOL-JEM2100F. The structural morphology of the nano-composite scaffolds was examined using scanning electron microscope (SEM). Scaffolds were sectioned into thin section with razor blade. The section were placed on aluminium stub and coated with platinum using JEOL JFC 1600 for 2 min at 10 mA before imaging. The average pore size was determined by measuring the size of 30 pores.

FTIR spectra of dried nBGC and nano-composite scaffolds were characterized using a FTIR spectrometer Perkin-Elmer RX1. Dried nBGC and nano-composite scaffolds were ground and mixed thoroughly with potassium bromide at a ratio of 1:5 (sample:KBr) and pelleted. The IR spectra of the pellets were then analyzed using Perkin-Elmer RX1 operating at range of 400–4000 cm^{-1}. XRD patterns of nano-composite scaffolds and nBGC were obtained at room temperature using a Panalytical XPERT PRO powder diffractometer (Cu Kα radiation) operating at a voltage of 40 kV. XRD were taken at 2θ angle range of 5–60° and the process parameters were scan step size 0.02 (2θ) and scan step time 0.05 s. Energy-dispersive X-ray spectroscopy (EDS) analysis was performed on JEOL JSM 6490 LA. A drop of nBGC/ethanol was placed on carbon tape coated stub. The sample was then platinum coated with JEOL JFC 1600 for 2 min for 10 mA.

2.5. Swelling studies

The swelling studies were performed in PBS (pH 7.4) at 37 °C. The dry weight of the scaffold was noted as W_i. Scaffolds were placed in PBS buffer solution (pH 7.4) at 37 °C for 1 h and then removed. The surface adsorbed water was removed by filter paper and wet weight was recorded W_W. The ratio of swelling was determined using the Eq. (1):

$$\text{Swelling ratio} = \frac{W_w - W_i}{W_i} \quad (1)$$

Swelling ratio was expressed as mean ± SD ($n = 3$).

2.6. Density studies

To determine the density of scaffold, three scaffolds from each batch was selected and measurement was done on Sartorius analytical balanced equipped with density determination kit (Sartorius YDK 01). Density measurements were done with ethanol as the displacement medium. Ethanol does not cause swelling or change in pore diameter hence ethanol was used as displacement medium. Density was recorded as mean ± SD ($n = 3$).

2.7. In vitro degradation studies

The degradation of the scaffold was studied in PBS (pH 7.4) medium containing lysozyme at 37 °C. Three scaffolds were immersed in lysozyme (10,000 U/ml) containing medium and incubated at 37 °C for 7 days. Initial weight of the scaffold was noted as W_i. After 7 days the scaffold was washed in deionised water to remove ions adsorbed on surface and freezed dried. The dry weight was noted as W_t. The degradation of scaffold was calculated using Eq. (2):

$$\text{Degradation}\,(\%) = \frac{W_i - W_t}{W_i} \times 100 \quad (2)$$

Degradation rate was recorded as mean ± SD ($n = 3$).

2.8. In vitro biomineralization studies

Three scaffolds of equal weight and shape was immersed in 1× simulated body fluid (SBF) [33] solution and then incubated at 37 °C in closed Falcon tube for 7 and 14 days. After specified time, the scaffolds were removed and washed three times with deionised water to remove adsorbed minerals. Finally the scaffolds were lyophilized, sectioned and viewed using SEM for mineralization.

2.9. Protein adsorption studies

Scaffolds of same shape and weight were placed in 96 well plates containing MEM + 10% FBS culture media. After 1 h incubation the scaffolds were rinsed with PBS solution thrice. Total protein was quantified using bicinchoninic acid (BCA) assay [34,35]. The principle of BCA assay is based on the reduction of Cu^{2+} to Cu^{1+}. The amount of reduction is proportional to the protein present. BCA reagent was added to each well and incubated for 30 min with the extract at 37 °C and the absorbance was read at wavelength of 562 nm. Scaffolds incubated in serum free medium were used as blank. Protein adsorption was plotted in optical density ($OD_{562\,nm}$) as mean ± SD ($n = 3$).

2.10. Cell studies

Cell studies were conducted using osteoblast-like cells (MG-63). Cell lines were maintained in the cell culture facility in MEM with 10% FBS and 100 U/ml penicillin–streptomycin. Cells were detached from the culture plate at 80–85% confluence and used for seeding on the scaffolds for investigating the cytocompatibility of scaffolds. Prior to cell seeding, scaffolds were sterilized using ethanol/UV treatment and incubated with culture medium for 1 h at 37 °C in a humidified incubator with 5% CO_2 and 85% humidity. Then the culture medium was removed completely from the scaffolds. Cells were seeded drop wise onto the top of the scaffolds (1×10^5 cells/100 μl of medium/scaffold), which fully absorbed the media, allowing cells to distribute throughout the scaffolds. Subsequently, the cell-seeded scaffolds were kept at 37 °C in a humidified incubator under standard culturing conditions for 4 h in order to allow the cells to attach to the scaffolds. After 4 h, the scaffolds were fed with additional culture medium.

2.11. Cytocompatability of the scaffolds

The viability of cells grown on the scaffolds was determined using the colorimetric MTT (3-(4,5-dimethylthiazol-2-yl)-2,5-diphenyltetrazolium bromide) assay. MTT assay measures the reduction of the tetrazolium component MTT by viable cells. Therefore, the level of the reduction of MTT into formazan can reflect the level of cell metabolism. For the assay, cells were then seeded on to 96 well plates at a density of 10^4 cells/well and were incubated under standard culturing conditions. Extract from the scaffolds were prepared by incubating the pre-sterilized scaffolds incubated in culture medium as per ISO specification 10993-5 (i.e. 60 cm^2 per 20 ml of medium for 24 h at 37 °C with agitation) and the medium with leachables was collected in a falcon tube. Culture media of the seeded cells were replaced after 24 h by the extract (media with the leachables). Cells were incubated on the extract for 24 and 48 h. After the incubation period, the extract was replaced by fresh media

containing 10% of MTT solution. Then the plates were incubated at 37 °C in humidified atmosphere for 4 h. Then the medium was removed, 100 μl of solubilization buffer (Triton-X 100, 0.1N HCl and isopropanol) was added to each well to dissolve the formazan crystals. The absorbance of the lysate was measured in a microplate reader (biotek) at a wavelength of 570 nm. Leachables from CG scaffolds incubated in culture medium were used as negative control, while Triton-X 100 treated medium was used as positive control.

Direct contact test was performed to show cytocompatability of the scaffolds placed in direct contact with cells. Cells were grown as monolayer on culture dishes and pre-sterilized scaffolds were placed and incubated for 24 h in direct contact to monolayer of cells. After the incubation period, scaffolds were removed from the monolayer of cells and images of the monolayer of cells were acquired with an inverted microscope (Leica) attached with a CCD camera.

2.12. Cell morphology on the scaffolds

Morphology and spreading pattern of cells on the scaffolds were evaluated using SEM after 48 h seeding. Scaffolds seeded with cells were fixed with 2.5% glutaraldehyde for 1 h, washed with PBS and dehydrated using alcohol gradient. Then the samples were platinum sputtered in vaccum (JEOL, JFC-1600, Japan), and examined using SEM (JEOL, JSM-6490LA, Japan).

2.13. Statistical analysis

All quantitative results were obtained from triplicate samples. Data was expressed as the mean ± SD. Statistical analysis was carried out using Student's two-tailed *t*-test. A value of $p < 0.05$ was considered to be statistically significant.

3. Results

3.1. Characterization

FTIR spectra of nBGC (Fig. 2) showed vibration bands at 467 and a shoulder at 1200 cm^{-1} which are assigned to Si–O–Si bending mode. The vibration band at 1070 cm^{-1} and a double peak at 607 and 567 cm^{-1} are due to the stretching vibration of phosphate groups [31]. The peaks at 2889 and 1637 cm^{-1} are attributed to CH stretching and O–H (molecular water) bending vibration band of PEG. This indicates that the PEG is present on the surface of nBGC nanoparticle [36,37]. The FTIR spectrum of CG scaffolds shows a peak at 1649 cm^{-1}, which corresponds to the primary amide groups

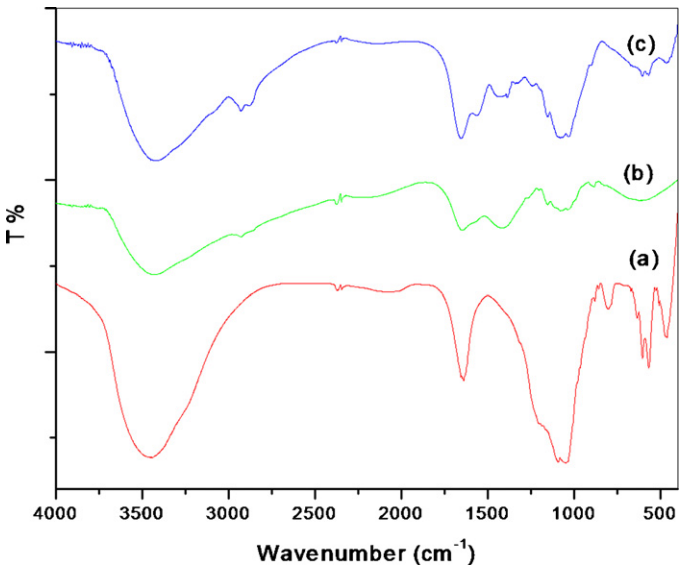

Fig. 2. FTIR spectra of (a) nBGC, (b) CG and (c) CG/nBGC scaffolds.

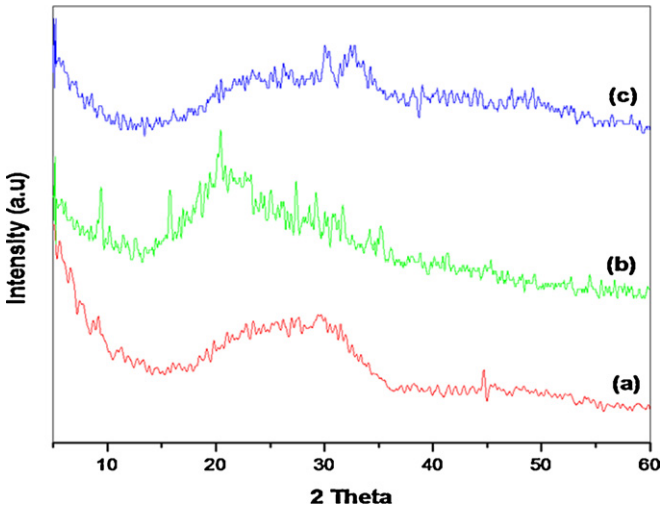

Fig. 3. XRD pattern of (a) nBGC, (b) CG and (c) CG/nBGC scaffolds.

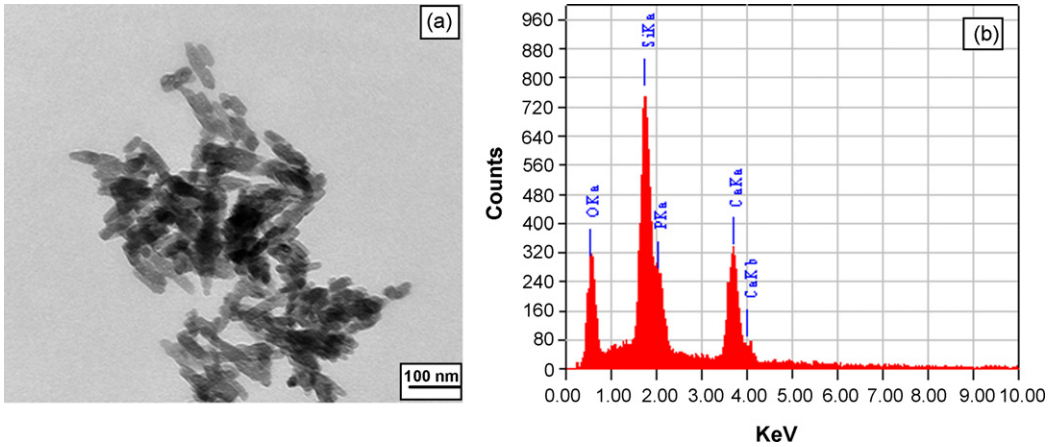

Fig. 4. (a) TEM micrograph showing the rod shape of nBGC nanoparticles with an average particle size below 100 nm. (b) EDS spectra of nBGC showing the peaks of Si, Ca, P and O. The atomic ratio of Si:Ca:P:O was 43:34:6:17 as determined by EDS.

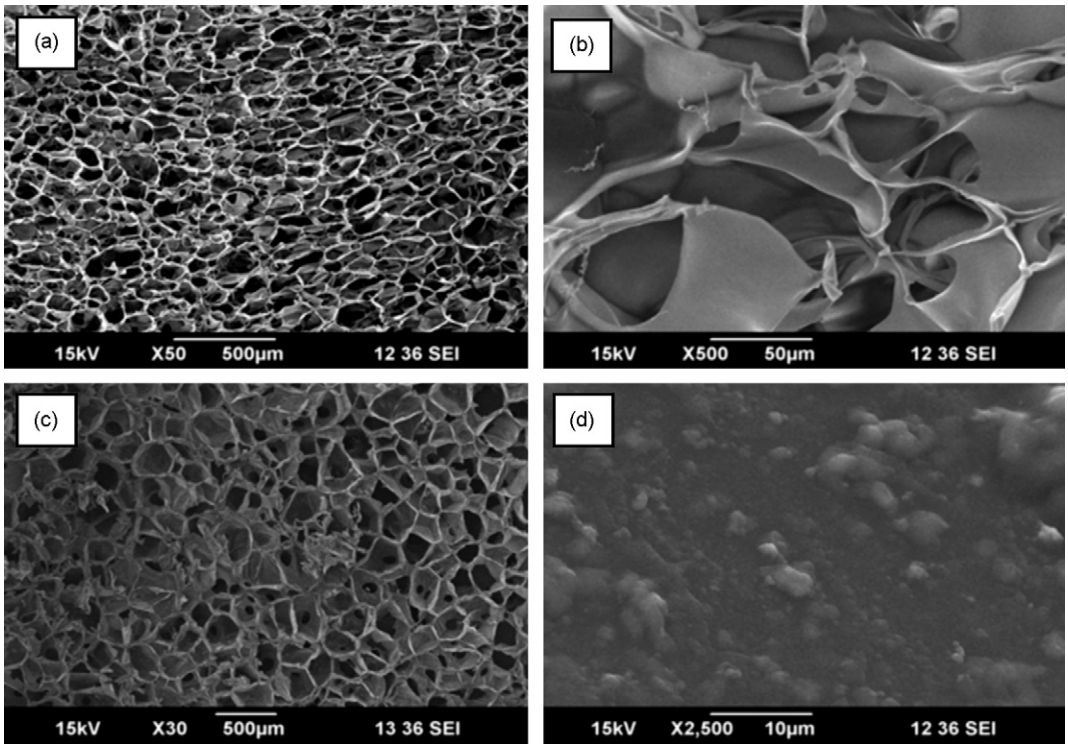

Fig. 5. SEM micrograph showing the macroporous microstructure of CG (a and b) and composite scaffold (c and d). Pore size ranged from 150 to 300 μm.

of chitosan. The peak at 1030 cm^{-1}, which is attributed to phosphate groups, was present in CG/nBGC scaffold while the peak at 1070 cm^{-1} was observed in CG, which was absent in CG/nBGC, and was assigned to C–O stretching of chitosan [38]. Fig. 3 shows the XRD pattern of nBGC calcined at 600 °C in air. The XRD studies (Fig. 3) confirmed that the calcinated glass generally existed in amorphous state and no diffraction peaks could be observed except a broad band between 15 and 40° (2θ) [31]. XRD of CG scaffold showed a peak at 21.5°, which is attributed to gelatin in the scaffold [17].

Fig. 4a shows the TEM micrograph of nBGC. The nBGC particles are rod shaped and the size of the particles was around 100 nm. The EDS spectrum (Fig. 4b) of nBGC shows the peaks of Ca, P, Si, and O. The atomic ratio of Si:Ca:P:O was found to be 43:34:6:17 as determined by EDS. EDS spectra of nano-composite scaffold also showed the presence of Si, Ca, P and O. SEM images showed that CG and CG/nBGc scaffolds (Fig. 5) pores were well interconnected and macroporous in nature. The nBGC particles were seen on the walls of the nano-composite scaffold and were uniformly dispersed in the matrix. Pore size of CG and CG/nBGC scaffold varied from 150 to 350 μm as measure by SEM. With the increasing concentration of chitosan the pore size decreased, which is in accordance with previously literature [39].

3.2. Density studies

Fig. 6 shows the density of the CG and CG/nBGC nano-composite scaffolds. The addition of nBGC decreases the density of the scaffold. This could be due to an increase in the porosity or pore size of the scaffolds, which decreases the density of the scaffold. It was also observed that the density of the scaffolds increased with increasing concentration of chitosan as reported in earlier works [39].

3.3. Swelling studies

Fig. 7 shows the swelling studies of CG and CG/nBGC nano-composite scaffolds. The incorporation of nBGC decreased the

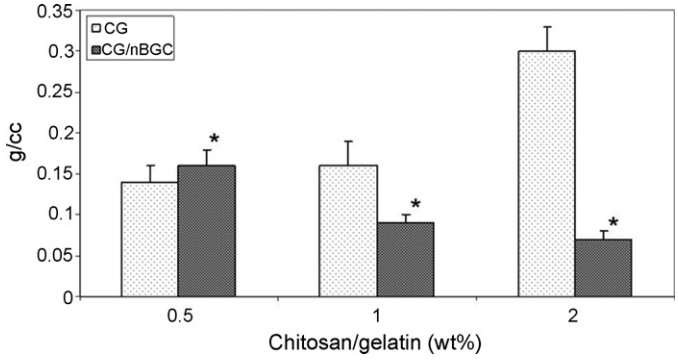

Fig. 6. The density of the CG and composite scaffolds. The addition of nBGC decreases the density of the scaffolds. *$p < 0.05$.

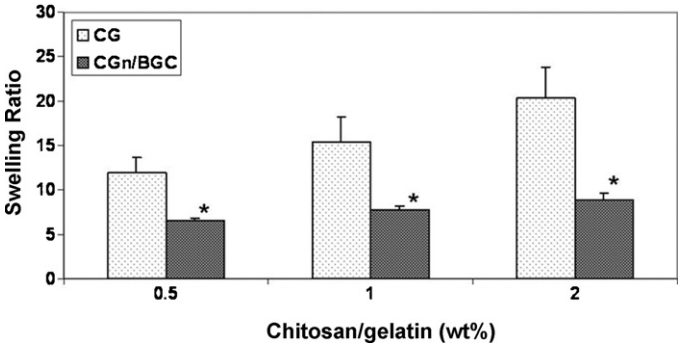

Fig. 7. Swelling behavior of the scaffolds shows that addition of nBGC decreased the swelling of the scaffolds. *$p < 0.05$.

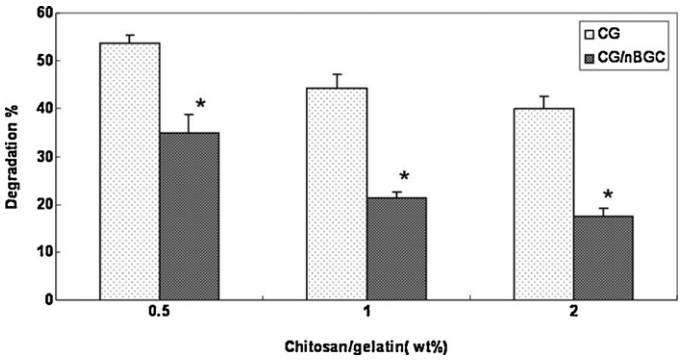

Fig. 8. *In vitro* degradation studies in lysozyme shows that a composite scaffold degrades more slowly than CG scaffolds. $^{*}p < 0.05$.

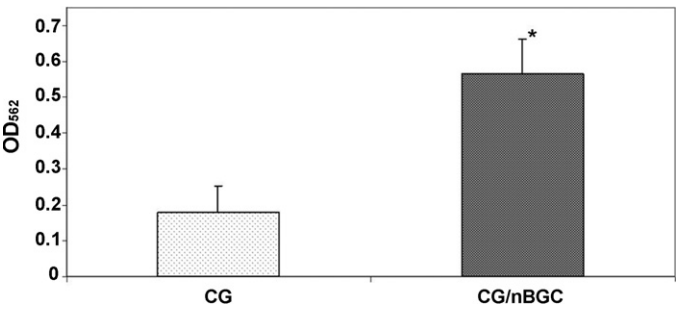

Fig. 9. Protein adsorption studies show that the composite scaffolds show a higher degree of protein adsorption compare to CG scaffolds.

swelling ability of the nano-composite scaffolds [17]. The swelling ability also decreased with increasing concentration of gelatin in the nano-composite scaffolds.

3.4. *In vitro degradation studies*

The *in vitro* biodegradation of the CG and CG/nBGC nano-composite scaffolds after 1 week of immersion in PBS containing lysozyme is represented in Fig. 8. Significant difference could be found in the degradation rate of the nano-composite scaffolds compared to CG scaffolds. The addition of nBGC significantly decreased the degradation rate of the nano-composite scaffolds. Higher the concentration of gelatin in the nano-composite scaffolds also decreased the degradation rate. Similar results have been reported earlier [17].

3.5. *Protein adsorption studies*

The protein adsorption studies showed a significant increase in protein adsorption on nano-composite scaffolds compared to CG scaffolds (Fig. 9).

3.6. *In vitro biominerialization studies*

The bioactivity studies of the CG/nBGC nano-composite scaffolds were performed in 1 × SBF incubated for 7 and 14 days. Fig. 10a and b shows the SEM micrograph of an apatite like layer on the surface of CG/nBGC after 7 days and Fig. 10c and d shows the SEM micrograph of an apatite like layer on the surface of CG/nBGC after 14 days. EDS spectra of mineralization showed the Ca/P ratio of 1.64 (Fig. 10e). This result shows the bioactive nature of the nano-composite scaffolds. The FTIR studies show a sharpening of peaks at 603 and 567 cm^{-1} corresponding to stretching vibration bands of phosphate group (Fig. 11a). XRD shows an increase in intensity of peak at 31.7° corresponding to hydroxyapatite (Fig. 11b).

3.7. *Cytocompatability studies*

Cytocompatibility of the CG and CG/nBGC nano-composite scaffolds were assessed using MTT assay and direct contact test. The OD values from the scaffolds did not show any decrease compared to the OD values from the negative control, after 24 and 48 h of incubation of the cells with the extract containing the leachables (Fig. 12a). This result suggests that there are no significant toxic leachables in the CG/nBGC composite scaffolds compared to CG scaffolds. Cells retained their characteristic cell morphology after 24 h of incubation in direct contact with the composite scaffolds (Fig. 12b). This result also supports the finding that nano-composite scaffolds are biocompatible.

3.8. *Cell attachment studies*

SEM micrographs was used to study the attachment, morphology and spreading of cells on the scaffolds. SEM images of cells

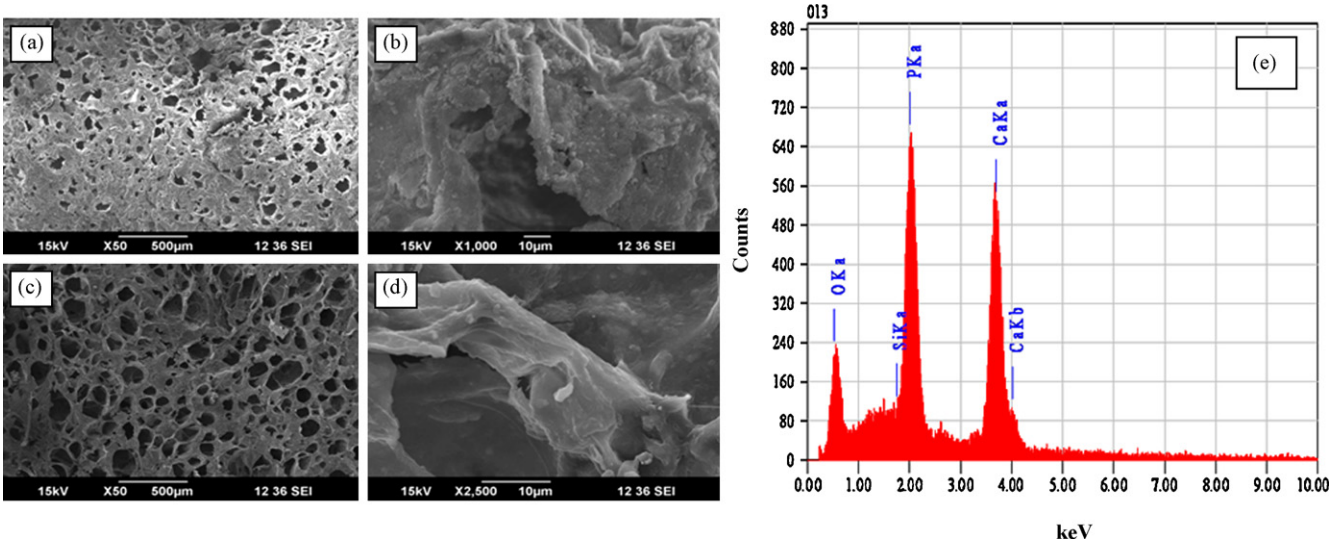

Fig. 10. (a and b) *In vitro* biomineralization studies on the composite scaffolds after 7 days and (c and d) after 14 days. (e) EDS spectra of apatite formed shows that the Ca/P ratio was 1.64.

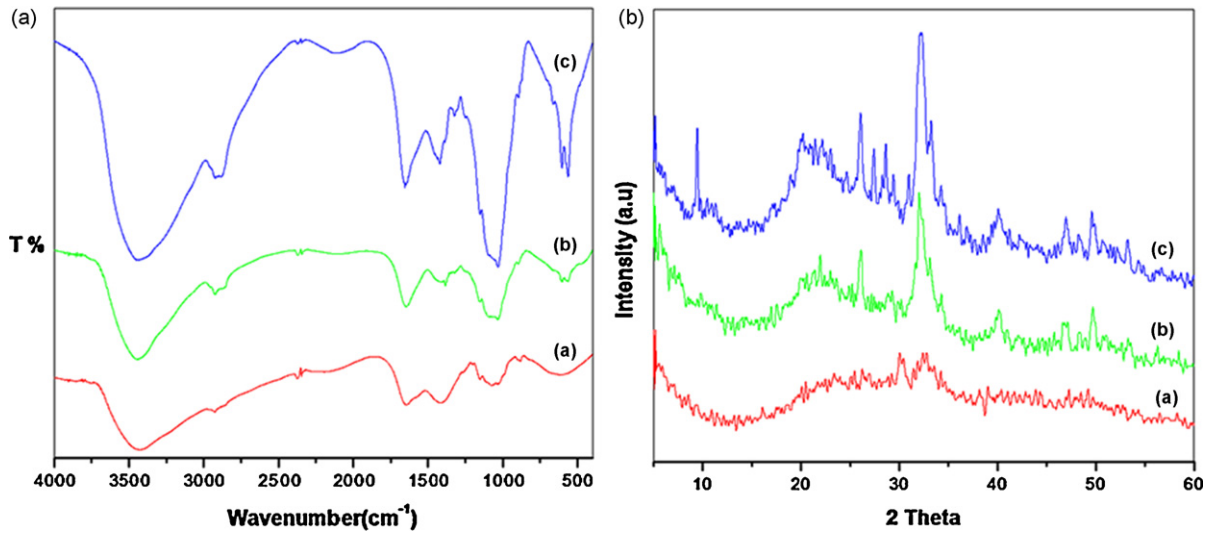

Fig. 11. (a) FTIR showing increases in intensity of phosphate peaks at 603 and 567 cm^{-1} after (a) control, (b) 7 days and (c) 14 days in SBF. (b) XRD showing an increase in intensity of HA peak at 31.7° after (a) control, (b) 7 days and (c) 14 days in SBF.

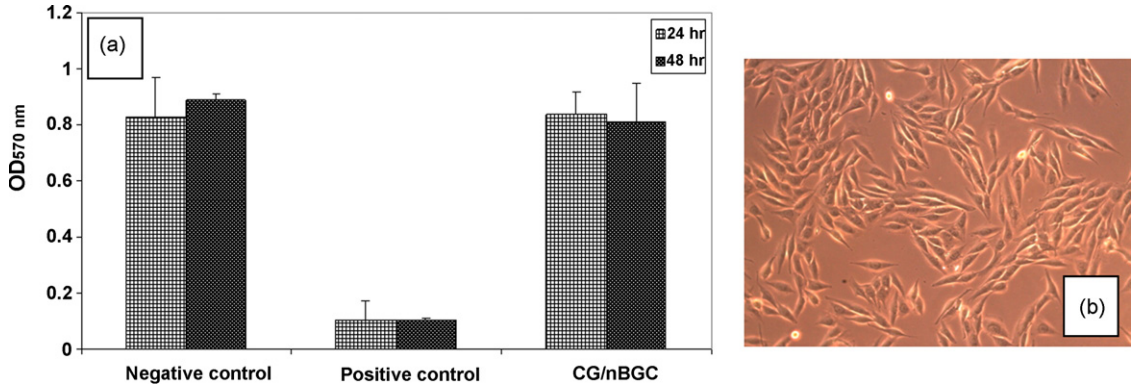

Fig. 12. (a) MTT assay showing biocompatibility of the composite scaffolds. (b) The morphology of cells grown in direct contact with cells.

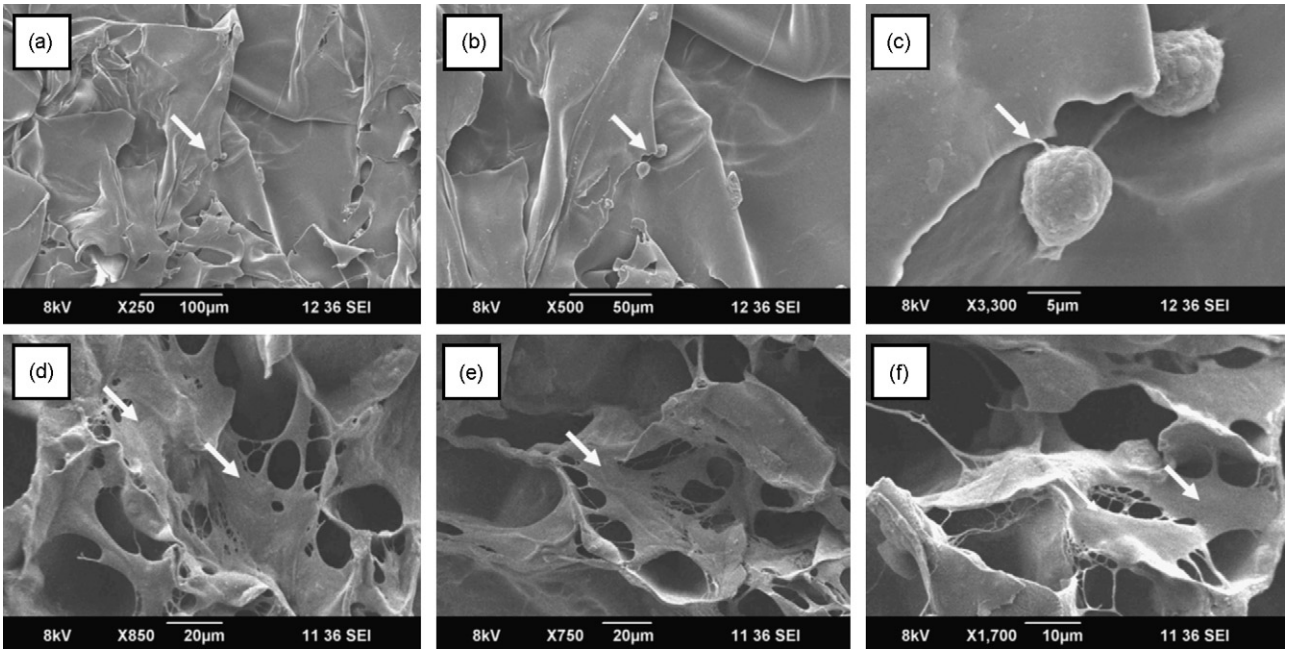

Fig. 13. The SEM image of MG-63 cells on the scaffolds after 48 h of incubation. Cells remained in a more or less round morphology (a–c) on CG scaffolds. However cells on the CG/nBGC nano-composite scaffolds (d–f, white arrows) showed well spread morphology.

incubated for 48 h on the scaffolds showed that cells attached and spread within the pore walls offered by the scaffolds. However, there were significant difference in morphology and spreading in a material dependent manner. After 48 h of incubation cells on the CG scaffolds remained in more or less round morphology (Fig. 13a–c). In contrast, cells on the nano-composite scaffolds exhibited a well spread morphology after the same period of incubation (Fig. 13d–f).

4. Discussions

FTIR studies showed the strong interaction between nBGC and CG network. In comparison to CG, CG/nBGC nano-composite scaffolds are characterized by three new absorption bands at 602 and 564 cm^{-1} which corresponds to the stretching vibration bands of P–O from $PO^{3-}{}_4$ and 467 cm^{-1} assigned to Si–O–Si bending mode as reported earlier [31]. The COOH group of gelatin in the scaffold may exist in the form of COO^- and an ionic or polar interaction could exist between COO^- and Ca^{2+} and also hydrogen bonds could also exist between $–NH_2$ and nBGC.

The pore size of the nano-composite scaffolds varied from 150 to 300 μm, which is adequate for cell migration into the interior regions of the scaffolds. Pores are necessary in bone tissue engineering for the migration and proliferation of osteoblasts and mesenchymal cells, as well as vascularization. The minimum recommended pore size for a scaffold is 100 μm as per reported literature [40]. But subsequent studies have been shown better osteogenesis for implants with pores >300 μm [40]. Relatively larger pores favour direct osteogenesis, since they allow vascularization and high oxygenation, while smaller pores result in osteochondral ossification, although the type of bone ingrowths depends on the biomaterial and the geometry of the pores.

Swelling studies showed a decrease in swelling rate with the addition of nBGC, which may be due to the strong interaction between nBGC and CG network. The hydrophilic groups of gelatin may be bonded with nBGC, which results in a reduction of the total number of hydrophilic groups. Swelling facilitate the infiltration of cells into the scaffolds in a three-dimensional fashion, during *in vitro* cell culture. Increase in the pore size allows cells to avail the maximum internal surface of the scaffolds. Samples showing higher degree of swelling will have a larger surface area/volume ratio thus allowing the samples to have the maximum probability of cell growth in a three-dimensional fashion. The increase in swelling also allows the samples to avail nutrients from culture media more effectively. However increase in swelling will also decrease the mechanical properties of the scaffold. Hence controlled swelling will be ideal for tissue engineering applications.

Degradation of the scaffolds is very important parameter in tissue engineering. Ideally the scaffolds should degrade as new tissue formation takes place. The β-1, 4 *N*-acetyl-glucosamine groups of chitosan chains can be hydrolyzed by lysozyme. Its degradation leads to the release of aminosugars, which can be incorporated into glycosaminoglycans and glycoprotein metabolic pathways, or excreted. The degradation rate was significantly decreased with the addition nBGC which may be due to neutralization of the acidic degradation products of chitosan by the alkali groups leaching from nBGC, thus reducing the degradation rate of the scaffold. The leach able products of bioactive glass systems are known to be alkaline in nature [41]. Nano-composite scaffolds with higher concentration of gelatin degrade faster. Gelatin being a hydrophilic polymer (presence of amide and carboxyl groups), the macromolecular chains of gelatin polymer hydrolyses quickly with the existence of water.

The BCA assay, which was used to determine protein adsorption, is one of the sensitive and applicable methods. The main advantages of BCA assay over other protein determination techniques include the easiness to use, the formation of a stable color complex, the less susceptibility to detergents and its application over a broad range of protein concentrations. Protein adsorption is known to influence the cell adhesion by adsorption of key adhesion molecules like fibronectin or vitronectin [42]. The increase in protein adsorption on the CG/nBGC nano-composite scaffolds can be due to the exposed nBGC on the scaffold surfaces, which increases the binding sites on the material surface for proteins, or promote an electrostatic interaction between the proteins and material surface and enhance adsorption of proteins [43].

The bioactivity studies showed *in vitro* mineralization ability of the nano-composite scaffolds. The mineral deposits were seen to increase with time of incubation. After 14 days the deposit uniformly forms a layer on the surface. The EDS studies showed that the surface deposition was apatite with Ca/P ratio of 1.64. It is close to the theoretical value of 1.67. The bioactivity of the nano-composite scaffolds allows for the formation of apatite layer, which results in a direct bonding of the implant with the bony defect. These results suggested that the nano-composite scaffolds are a suitable material for tissue engineering applications.

The cell cytotoxicity was assessed by MTT assay and the results showed no significant cytotoxicity compared to the control used as reference. These results suggest that cell viability is not affected by addition of nBGC nanoparticles. nBGC nanoparticles can cause alkalization of culture medium due to the leachable products from nBGC. This may cause an increase in Ca^{2+} ions in culture medium. The increased intracellular Ca^{2+} ions level may induce apoptosis of the cells. However the results show no significant change in cytotoxicity between the controls and samples indicating that composite scaffolds are biocompatible.

Cell attachment studies showed that the CG/nBGC nano-composite scaffold significantly increased the cell attachment when compared to CG scaffolds. The SEM micrographs show flatened morphology of MG-63 cells and forming bridges between pores. Previous works by Blaker et al. [44] have shown similar results with MG-63 cell line. The result indicates that the nano-composite scaffolds might be suitable for alveolar bone tissue engineering. The higher attachment on nano-composite scaffolds may be due increase in surface area and roughness of the surface. It is known that surface topology could play a role in cell attachment on implants [45–47]. An increase in surface area allows maximum area for cell attachment and nano-surfaces have larger surface area to volume ratio. This larger surface area may play a role in increasing protein adsorption especially adhesive proteins. Further studies are needed to find out the specific protein adsorbed on the scaffold surface and their role cell attachment on nano-composite scaffold.

5. Conclusions

Porous biodegradable CG/nBGC nano-composite scaffolds with sufficient microporosity for cell infiltration can be obtained through freezing and lyophilization technique. The swelling and degradation rate of the nano-composite scaffolds decreased with addition of nBGC and protein adsorption increased. The nano-composite scaffolds shows good bioactivity and better cell attachment and spreading compared to CG scaffolds. Therefore we concluded that CG/nBGC nano-composite scaffolds appear to be a promising nano-composite material for alveolar bone tissue engineering.

Acknowledgements

The Department of Science and Technology, Government of India supported this work, under a centre grant of the Nanoscience and Nanotechnology Initiative program monitored by Dr. C.N.R.

Rao. The authors are thankful to Prof. Greta R. Patzke, Institute of Inorganic Chemistry, University of Zurich for helping in TEM studies. The authors are also thankful to Mr. Sajin. P. Ravi for his help in SEM studies.

References

[1] G.C. Armitage, Periodontal diagnoses classification of periodontal diseases, Periodontology 34 (2004) 9–21.
[2] P.M. Bartold, C.G. McCulloc, A.S. Narayanan, S. Pitaru, Tissue engineering: a new paradigm for periodontal regeneration based on molecular and cell biology, Periodontology 24 (2000) 253–269.
[3] P.M. Bartold, Y. Xiao, S.P. Lyngstaadas, M.L. Paine, M.L. Snead, Principles and applications of cell delivery systems for periodontal regeneration, Periodontology 41 (2006) 123–135.
[4] R.A.A. Muzzarelli, V. Baldassarre, F. Conti, P. Ferrara, G. Biagini, Biological activity of chitosan: ultrastructural study, Biomaterials 9 (1988) 247–252.
[5] R.A.A. Muzzarelli, G. Giacomelli, The blood anticoagulant activity of *N*-carboxymethylchitosan trisulfate, Carbohydr. Polym. 9 (1987) 87–96.
[6] R.A.A. Muzzarelli, Chitins and chitosans for the repair of wounded skin, nerve, cartilage and bone, Carbohydr. Polym. 76 (2009) 167–182.
[7] R. Jayakumar, N. Nwe, S. Tokura, H. Tamura, Sulfated chitin and chitosan as novel biomaterials, Int. J. Biol. Macromol. 40 (2007) 175–181.
[8] R. Jayakumar, M. Prabaharan, R.L. Reis, J.F. Mano, Graft copolymerized chitosan-present status and applications, Carbohydr. Polym. 62 (2005) 142–158.
[9] R.A.A. Muzzarelli, R. Tarsi, O. Filippini, E. Giovanetti, G. Biagini, Antimicrobial properties of *N*-carboxybutyl chitosan, Antimicrob. Agents Chemother. 34 (1990) 2019–2023.
[10] Y.F. Zhang, X.R. Cheng, Y. Chen, B. Shi, X.H. Chen, D.X. Xu, J. Ke., Three-dimensional nanohydroxyapatite/chitosan scaffolds as potential tissue engineered periodontal tissue, J. Biomater. Appl. 21 (2007) 333–349.
[11] F. Zhao, W.L. Grayson, T. Ma, B. Bunnell, W.W. Lu, Effects of hydroxyapatite in 3D chitosan–gelatin polymer network on human mesenchymal stem cell construct development, Biomaterials 27 (2006) 1859–1867.
[12] I. Manjubala, S. Scheler, J. Bossert, K.D. Jandt, Mineralisation of chitosan scaffolds with nano-apatite formation by double diffusion technique, Acta Biomater. 2 (2006) 75–84.
[13] Y. Takahashi, M. Yamamoto, Y. Tabata, Osteogenic differentiation of mesenchymal stem cells in biodegradable sponges composed of gelatin and, β-tricalcium phosphate, Biomaterials 26 (2005) 3587–3596.
[14] H.H. Xu, C.G. Simon, Fast setting calcium phosphate-chitosan scaffold: mechanical properties and biocompatibility, Biomaterials 26 (2005) 1337–1348.
[15] H. Jiankang, L. Dichen, L. Yaxiong, Y. Bo, Z. Hanxiang, L. Qin, L. Bingheng, L. Yi, Preparation of chitosan–gelatin hybrid scaffolds with well-organized microstructures for hepatic tissue engineering, Acta Biomater. 5 (2009) 453–461.
[16] Z. Li, H.R. Ramay, D.K. Hauch, D. Xiao, M. Zhang, Chitosan–alginate hybrid scaffolds for bone tissue engineering, Biomaterials 26 (2005) 3919–3928.
[17] J.P. Zheng, C.Z. Wang, X.X. Wang, H.Y. Wang, H. Zhuang, K.D. Yao, Preparation of biomimetic three-dimensional gelatin/montmorillonite-chitosan scaffolds for tissue engineering, React. Func. Polym. 67 (2007) 780–788.
[18] A.G. Word, A. Courts, The Science and Technology of Gelatin, Academic Press, London, 1977.
[19] L.L. Hench, Bioceramics: from concept to clinic, J. Am. Ceram. Soc. 74 (1991) 1487–1510.
[20] A. El-Ghannam, P. Ducheyne, I.M. Shapiroc, Formation of surface reaction products on bioactive glass and their effects on the expression of the osteoblastic phenotype and the deposition of mineralized extracellular matrix, Biomaterials 18 (1997) 295–303.
[21] S. Foppiano, S.J. Marshall, G.W. Marshall, E. Saiz, A.P. Tomsia, Bioactive glass coatings affect the behaviour of osteoblast-like cells, Acta Biomater. 3 (2007) 765–771.
[22] P. Valerio, M.M. Pereira, A.M. Goes, F. Leite, The effect of ionic products from bioactive glass dissolution on osteoblast proliferation and collagen production, Biomaterials 25 (2004) 2941–2948.
[23] L.L. Hench, Genetic design of bioactive glass, J. Eur. Ceram. Soc. 29 (2009) 1257–1265.
[24] M. Bosetti, M. Cannas, The effect of bioactive glasses on bone marrow stromal cells differentiation, Biomaterials 26 (2005) 3873–3879.
[25] I.D. Xynos, A.J. Edga, L.D.K. Buttery, L.L. Hench, J.M. Polak, Ionic products of bioactive glass dissolution increase proliferation of human osteoblasts and induce insulin-like growth factor II mRNA expression and protein synthesis, Biochem. Biophys. Res. Commun. 276 (2000) 461–465.
[26] R.M. Day, A.R. Boccaccini, S. Shurey, J.A. Roether, A. Forbes, L.L. Hench, S.M. Gabe, Assessment of polyglycolic acid mesh and bioactive glass for soft-tissue engineering scaffolds, Biomaterials 25 (2004) 5857–5866.
[27] S. Verrier, J.J. Blaker, M. Maquet, L.L. Hench, R.A. Boccaccinia, PDLLA/bioglass composites for soft-tissue and hard-tissue engineering: an in vitro cell biology assessment, Biomaterials 25 (2004) 3013–3021.
[28] T. Kokubo, Bioactive glass ceramics: properties and applications, Biomaterials 12 (1991) 155–163.
[29] D.L. Wheeler, M.J. Montfort, S.W. McLoughlin, Differential healing response of bone adjacent to porous implant coated with hydroxyapatite and bioactive glass, J. Biomed. Mater. Res. 55 (2000) 603–612.
[30] M. Vogel, C. Voigt, U.M. Gross, C.M. Mai, In vivo comparison of bioactive glass particles in rabbits, Biomaterials 22 (2001) 357–362.
[31] W. Xia, J. Chang, Preparation and characterization of nano-bioactive-glasses (NBG) by a quick alkali-mediated sol–gel method, Mater. Lett. 61 (2007) 3251–3253.
[32] T.J. Webster, C. Ergun, R.H. Doremus, R.W. Siegel, R. Bizios, Enhanced functions of osteoblasts on nanophase ceramics, Biomaterials 21 (2000) 1803–1810.
[33] T. Kokubo, H. Takadama, How useful is SBF in predicting in-vivo bone activity? Biomaterials 27 (2006) 2907–2915.
[34] J.M. Walker, The bicinchoninic acid (BCA) assay for protein quantitation, Methods Mol. Biol. (1994).
[35] S.F. Hulbert, F.A. Young, R.S. Mathews, J.J. Klawitter, C.D. Talbert, F.H. Stelling, Potential of ceramic materials as permanently implantable skeletal prostheses, J. Biomater. Appl. 4 (1970) 433–456.
[36] H. Mansur, H. Costa, Nanostructured poly(vinyl alcohol)/bioactive glass and poly (vinylalcohol)/chitosan/bioactive glass hybrid scaffolds for biomedical applications, Chem. Eng. J. 137 (2008) 72–83.
[37] S. Petrova, S. Miloshev, R. Mateva, I. Illev, Synthesis of amphiphilic PEG–PCL–PEG triblock copolymer, J Univ. Chem. Technol. Metall. 43 (2008) 199–204.
[38] J. Li, Y. Dou, J. Yang, Y. Yin, H. Zhang, F. Yao, H. Wang, Y. Yao, Surface characterization and biocompatibility of micro- and nano-hydroxyapatite/chitosan–gelatin network films, Mater. Sci. Eng. C29 (2009) 1207–1215.
[39] J.S. Mao, L.G. Zhao, Y.J. Yin, K.D. Yao, Structure and properties of bilayer chitosan–gelatin scaffolds, Biomaterials 24 (2003) 1067–1074.
[40] V. Karageorgiou, D. Kaplan, Porosity of 3D biomaterial scaffolds and osteogenesis, Biomaterials 26 (2005) 5474–5491.
[41] I.A. Silver, J. Deas, M. Erecinska, Interactions of bioactive glasses with osteoblasts in vitro: effects of 45S5 bioglass, and 58S and 77S bioactive glasses on metabolism, intracellular ion concentrations and cell viability, Biomaterials 22 (2001) 175–185.
[42] H.W. Kim, H.E. Kim, V. Salih, Stimulation of osteoblast responses to biomimetic nanocomposites of gelatin–hydroxyapatite for tissue engineering scaffolds, Biomaterials 26 (2005) 5221–5230.
[43] P. Linez-Bataillon, F. Monchau, M. Bigerelle, H.F. Hildebrand, In vitro MC3T3 osteoblast adhesion with respect to surface roughness of Ti6Al4V substrates, Biomol. Eng. 19 (2002) 133–141.
[44] J.J. Blaker, J.E. Gough, V. Maquet, I. Notingher, A.R. Boccaccini1., *In-vitro* evaluation of novel bioactive composites based on Bioglass®-filled polylactide foams for bone tissue engineering scaffolds, J. Biomed. Mater. Res. A 67 (2003) 1401–1411.
[45] G. Lauer, M. Wiedmann-Al-Ahmad, J.E. Otten, U. Hubner, R. Schmelzeisen, W. Schilli, The titanium surface texture effects adherence and growth of human gingival keratinocytes and human maxillar osteoblast-like cells in vitro, Biomaterials 22 (2001) 2799–2809.
[46] M.J. Dalby, D. McCloy, M. Robertson, C.D.W. Wilkinson, R.C. Oreffo, Osteoprogenitor response to defined topographies with nanoscale depths, Biomaterials 27 (2006) 1306–1315.
[47] S.R. Chastain, A.K. Kundu, S. Dhar, J.W. Calvert, A.J. Putnam, Adhesion of mesenchymal stem cells to polymer scaffolds occurs via distinct ECM ligands and controls their osteogenic differentiation, J. Biomed. Mater. Res. 78A (2006) 73–85.